HIGH CHROME REFRACTORY CHARACTERIZATION: PART I. IMPACT OF MELT REDUCTION/OXIDATION (REDOX) ON THE CORROSION MECHANISM

C. M. Jantzen,‡ K.J. Imrich,† K.G.Brown,* and J.B. Pickettƒ
Savannah River National Laboratory
Savannah River Nuclear Solutions
Aiken, SC 29808

Keywords: refractory, corrosion, melter life, melter accumulation

ABSTRACT

High Cr_2O_3 containing Monofrax™ K-3 is a robust refractory that is used in the fiberglass industry and used in radioactive waste glass melters worldwide. Monofrax™ K-3 is tolerant of transition metal oxides but contains highly reduced solid solutions of spinels, i.e. $(Mg,Fe^{2+})(Al,Cr)_2O_3$. Conversely, many of the waste feeds being processed are highly oxidizing. The K-3 refractory corrosion was tested in sealed crucibles starting with slurried melter feed instead of pre-reacted glass called for by ASTM C621. Testing the refractory coupon during the feed-to-glass conversion exposes the refractory to the oxidizing and reducing species being released during vitrification, e.g. NO_3^-, NO_2^-, CO_2, CO, O_2. Corrosion rates measured in highly oxidizing (high nitrate) feeds were ~1.8-2.8 times higher than those determined using pre-reacted glass or reduced feeds. Confirmatory corrosion rates were measured on Monofrax™ K-3 coupons immersed in oxidizing feed in a 1/100th scale HLW pilot-scale melter. Corrosion is heterogeneous or incongruent as Ni and Fe in the waste glass exchange with Mg and Al in the refractory. An insoluble $NiFe_2O_4$ spinel corrosion product is formed that can build up a protective layer along the refractory walls or spall and settle to the melter floor depending on melt pool convection/agitation.

1.0 INTRODUCTION

Monofrax™ K-3 refractory has been used to line the High Level Waste (HLW) melters at the Savannah River Site (SRS), e.g. the Defense Waste Processing Facility (DWPF), and at West Valley Nuclear Services (WVNS). In addition, Monofrax™ K-3 was the refractory lining used in Duratek's Duramelter 5000 in the SRS M-Area facility where high nitrate Low Level Mixed Waste (LLMW) waste was vitrified. Monofrax™ K-3 has also been used in Hanford's HLW and Low Activity Waste (LAW) melter designs. In addition, Monofrax™ K-3 is being used in HLW melters in Japan.

‡ carol.jantzen@srnl.doe.gov; Fellow and Distingusihed Life Member American Ceramic Society
† ken.imrich@srnl.doe.gov
* current address Department of Civil and Environmental Engineering,Vanderbilt University, Nashville, TN 37235, kevin.g.brown@vanderbilt.edu
ƒ pickett.john@bellsouth.net, retired Savannah River Site, Fellow American Ceramic Society

Previous scale melter testing of the Monofrax™ K-3 refractory at the Savannah River National Laboratory (SRNL) had been performed using only reducing feeds containing minimal concentration of oxidizers (nitrate and nitrite). [1] Currently, reduced feeds are being processed in the DWPF but in 1996 during DWPF non-radioactive startup the feeds were very oxidizing (Table 1). The feeds that were vitrified in the SRS M-Area facility and in the WVNS HLW melter were also highly oxidizing. Highly oxidizing HLW and LAW wastes will also be vitrified at Hanford at the Waste Treatment and Immobilization Plant (WTP).[2] The WTP flowsheet is oxidizing due to (1) the high nitrate content of the feeds which gives off oxygen during denitration in the melter, and (2) the intent to bubble air into the melt to increase throughput. The characterization and corrosion data, the modeling of spinel accumulation from the refractory under various REDOX conditions, and validation of the depth of the spinel deposits from the non-radioactive startup testing in DWPF when oxidizing feeds were processed are, therefore, relevant to the impending startup of the WTP. The relative nitrate and nitrite concentrations of the wastes at the SRS, WVNS and WTP are compared in Table 1 . All of the melters described in Table 1 were lined with Monofrax™ K-3 refractory.

2.0 BACKGROUND

2.1 Corrosion Mechanisms

Melter refractory can be corroded by the glass, steel, or slag[f] being processed at the melt temperature [3,4]. Attack of refractories involves chemical wear (corrosion) as well physical/mechanical wear, i.e. erosion and abrasion. These processes may interact synergistically. [4] To understand the corrosion mechanisms the (1) refractory microstructure including the composition and textures of the individual phases and how they are bonded to each other, (2) melt composition and viscosity, and (3) the wetting of the refractory by the glass or slag and their interaction.[4] If the dissolution occurs by the direct solution of all the refractory phases into the corroding glass, it is termed direct, homogeneous, or congruent dissolution. If, however, one or more phases are preferentially dissolved, it is termed indirect, incongruent, or heterogeneous dissolution. Heterogeneous dissolution generally forms one or more new crystalline phases at the solid-liquid interface.[4] If the crystalline phase formed is not completely soluble in the glass or slag, it may form an impenetrable barrier so that, after its formation, further attack is prevented or slowed. [5] Thus, an "in-situ" refractory surface is formed from the corrosion products provided that the products are not removed by melt stirring, bubbling, or other agitation. This type of "in-situ" refractory surface has been observed in pilot scale HLW melters lined with Monofrax™ K-3 where only natural melt convection was active. [6]

The driving force for refractory corrosion is the difference between the saturated and bulk concentration of the refractory in the glass, i.e. during chemical attack, the system attempts to attain thermodynamic equilibrium between the refractory (solute) and the glass melt (solvent).[7] In order to establish equilibrium at the glass/ceramic interface a where a boundary layer forms. If the boundary layer composition differs from that of the bulk glass, melt diffusion will continue until either all solid has dissolved or the melt achieves equilibrium with the interface composition. Oxide

[f] Slag is generally considered a partially vitreous by-product of the process of smelting. When ores are smelted, the slag produced is usually a mixture of metal oxides and silicon dioxide. Throughout this document, slag is defined as a mixture of transition metal spinels which may come from crystallization of the melt or spalling of refractory corrosion products, glass, and other crystalline silicate reaction products.

dissolution rates in glass melts depend on four key factors: (1) diffusion rate of refractory components into the melt, (2) solubility of the refractory within the melt, (3) mobility of the reacting species in the melt, and (4) mobility of the dissolved refractory in the melt. [7] Thus the most desirable refractory would then be one that has the lowest solubility in the glass.

The dominant phase in high Cr_2O_3 refractories like Monofrax™ K-3 is a complex solid solution of various spinels. The spinel phases are mixtures of the four end member spinels $(Mg,Fe)O\bullet(Al,Cr)_2O_3$ and some SiO_2.[4,8,9,10,11] Although Cr_2O_3 is poorly soluble in DWPF glass (see Appendix A), other components of the Monofrax™ K-3 refractory have been found to be soluble in HLW waste glass [10,11] and reduced Fe species in the refractory can easily oxidize when in contact with oxidizing feeds in the melter.

High Cr_2O_3 refractories are commonly used in steel manufacturing, in the commercial glass industry, and in the nuclear/hazardous waste vitrification industry [8,9,12,13,14,15]. The corrosion mechanisms by which high Cr_2O_3 refractories have been found to degrade in the steel industry are outlined by Muan and Osborn [13]. The causes include fluctuating temperature, fluctuating oxygen partial pressure (pO_2), and poor resistance to attack of the refractory by molten iron oxide in the steel, slag, or glass being melted.

One mechanism by which high chrome refractories can degrade is by some component in the refractory combining with some component in the material being melted and forming a low melting eutectic liquid.[13] Most high Cr_2O_3 refractories contain some SiO_2 and considerable MgO. The addition of MgO improves the temperature resistance of the refractory when exposed to calcium silicate slags.[13] Significant concentrations of FeO, Fe_2O_3 and Al_2O_3 decrease the refractoriness of high Cr_2O_3 refractories as the ternary phase diagrams for the $FeO\text{-}Al_2O_3\text{-}SiO_2$ system and the $Fe_2O_3\text{-}Al_2O_3\text{-}SiO_2$ systems indicate low melting eutectic temperatures, e.g. 1083°C and ~1350°C, respectively.[13] These low melting eutectics allow the molten slag or glass and refractory to react at temperatures as low as 1083°C.

A second mechanism by which chrome refractories can degrade, such as on melter roofs and walls, can be brought about by solid state phase changes. Layers on the order of 2.54 cm in thickness may spall or peel off.[13] In other instances, refractory disintegration can occur.[13] The peeling off of layers is believed to be due to a "bursting expansion" accompanying iron oxide (Fe_2O_3) absorption by the spinel grains of the chrome spinel in the refractory.[13] When iron oxide goes into solid solution in the spinel, swelling occurs as the porosity is increased. Growth of MgO crystals can also cause spalling. Other factors that play a role in the peeling of chrome refractories are stresses associated with temperature changes and thermal shock.[13]

2.2 Impact of Oxidizing vs. Reducing and Static vs. Dynamic Melts

Testing of fuse-cast chrome-alumina refractory used in the fiberglass industry has been carried out in both reducing and oxidizing glasses and with and without agitation.[16] The refractory was tested under static and rotating conditions [16] in a borosilicate melt at a temperature of 1316°C. Under static conditions, the glass adjacent to the refractory became saturated with the refractory components and further dissolution was retarded, i.e. the saturated layer was protective of the refractory. This is designated as a Type III "in situ"

refractory by Lee et.al.[17] where the refractories and glass form a reaction layer that can be protective. However, during melt rotation or stirring, the saturated protective layer was removed from the refractory wall and replaced by fresh glass melt.[16] The fresh glass melt in contact with the refractory caused increased corrosion.

The range of glass REDOX tested in the fiberglass experiments of Cooper and Nicholson [16] as indicated by the $Fe^{+2}/\sum Fe$ ratio was 0.24 to 0.71. Glasses were oxidized by adding $NaNO_2$ to the feed since the high melting temperature, 1316°C, otherwise would stabilize reduced glass, e.g. a glass with no $NaNO_2$ had an $Fe^{+2}/\sum Fe$ ratio of 0.71. The testing* indicated that, when there was no glass flow, the REDOX conditions of the glass appeared to have no influence on the corrosion of the fusion cast alumina-chrome refractories. Where glass was flowing (low flow), as during natural melter convection, the REDOX condition of the glass was found to affect the corrosion rate. The data of Cooper and Nicholson also indicated that the REDOX condition of the glass had the greatest influence on refractory corrosion at low glass flow rates. At increased flow rates, glass flow becomes the controlling factor in refractory corrosion. The conclusion of the study indicated that the addition of a reducing agent to fiberglass compositions would decrease the wear rate of fusion-cast refractories. It should also be noted that testing of high Cr_2O_3 refractories at the Carborundum Company [10] and the data of Muan, et. al. [13] demonstrate that refractory corrosion rates are higher with glasses containing >0.2 wt% Fe as oxidized Fe_2O_3. Miller and Steggs [10] determined that the Al_2O_3 phase of the Monofrax™ K-3 brick was much more vulnerable to solution in glass than the chrome (Cr_2O_3) phase. This result is in agreement with the findings of Muan and Obsorn [13] for the degradation of Cr_2O_3 refractories in molten calcium silicate slags. Miller and Steggs also identified the Monofrax™ K-3 corrosion mechanism in DWPF type glasses as being a strong function of the nickel oxide and iron oxide (Fe_2O_3) in the glass where Ni and Fe in the glass exchange with Mg and Al in the refractory. A Ni-Cr-Fe spinel is formed as a reaction product [12].

2.3 DWPF Materials of Construction Testing In Pre-Reacted Glass

The ASTM C621 test protocol [18] uses pre-reacted glass and measures an overall corrosion rate which is defined as "the average loss of material". For the corrosion of K-3, the corrosion rate was expressed as two different rates: an "average loss of material" and a "total penetration depth." [19,20,21] The two different rates were defined to correspond to two different reaction mechanisms which occurred between the specimen and the molten glass: (1) a "corrosion" reaction mechanism which resulted in a change in the dimensions of the specimen (corresponding to the "average loss of material") and (2) "selective penetration" of a corrosion front into the material forming a new reaction layer (corresponding to the "total penetration depth").

The corrosion rate of both refractory [3,13,9] and metal [9,22] melter materials of construction are dependent on the melt fugacity, i.e. REDOX. This dependency on melt fugacity is well documented because both the refractory and the metals are composed of REDOX active species such as Cr, Mn, Ni, and Fe. However, the refractory and electrode corrosion tests done in support of the DWPF materials selection were performed in crucibles

* The data in this study are presented graphically and the penetration rates are not tabulated.

with simulated DWPF glass made from component oxides or pre-reacted glass rather than from the reducing waste feeds. Therefore, the effects of oxidizing or reducing feed additives on the refractories and metals were not fully evaluated.

Early materials of construction testing for the DWPF [18,19,19,21,23,24] indicated that Inconel®690 and Monofrax™ K-3 were the best candidates. Later corrosion testing in simulated waste glass confirmed that Monofrax™ K-3 was the most durable refractory tested [19,21]. Corrosion testing in glasses made with real waste indicated that the real waste glass was 2-3 times more corrosive than simulated wastes [24].

Corrosion testing also indicated that both Inconel®690 and K-3 refractory corrosion was greatly impacted by the amount of Na_2O in a given waste glass.[21] However, these initial refractory coupon tests [18,19,19,21,23,24,25] in crucibles did not address the effects of feed additives such as formic acid and/or nitric acid on the corrosion of the Monofrax™ K-3 refractory because the ASTM test calls for the usage of prefabricated glass. At the time the preliminary materials of construction testing was performed for the DWPF a reducing flowsheet (formic acid only) was planned to control the melt pool REDOX at an $Fe^{2+}/\Sigma Fe$ of ~0.2 to control volatilization of radionuclides and foaming.[26]

2.4 DWPF Materials of Construction Testing in Oxidized Feeds

During the first 1.75 years of non-radioactive DWPF operation, simulated oxidizing (nitric acid only) feeds were slurry fed and processed. An accumulation of ~0.06m (2.5") of melter bottom deposits was noted after the first 1.75 years. This deposit accumulation rate (meters/year) was more rapid than previously experienced in large pilot scale testing with slurry feeding and reducing flowsheets. Since the DWPF was initially operating using an oxidizing flowsheet compared to the reduced flowsheets tested in various pilot scale melters, the following studies were performed:

1. analyze the REDOX of the K-3 refractory
2. analyze the K-3 for the presence of trace components
3. analyze the phase assemblages present in the K-3 refractory to determine the corrosion mechanism and decomposition products when in contact with molten glass
4. measure the K-3 refractory corrosion in a SRNL165 glass average waste composition simulated glass as a control to reproduce the corrosion rates reported by previous researchers during the selection of the K-3 refractory for the DWPF
5. measure and compare the K-3 refractory corrosion in the pre-reacted glass as a control and in oxidizing feeds in sealed crucible tests
6. measure the K-3 refractory corrosion in oxidizing feeds in the SRNL 774-A mini-melter
7. determine if oxidizing feeds are causing accelerated chemical attack of the K-3 refractory
8. estimate the rate and the thermodynamic driving forces for K-3 refractory corrosion
9. analyze the composition and phase identification of the DWPF bottom deposits

10. estimate spinel accumulation rates on the floor of the DWPF melter for oxidizing and reducing flowsheets from measured corrosion rates in crucible studies and pilot scale melters
11. verify the calculated depth of the deposits with the depth measured by rodding the DWPF melter after 1.75 years of operation.

Part I of this study addresses the results from items 1-8 while Part II [1] of this study addresses items 9-11 including summarizing the melter accumulation deposits observed in pilot scale melters at SRS including the 1.75 years of non-radioactive processing in the full scale DWPF.

3.0 EXPERIMENTAL

A brick of Monofrax™ K-3 refractory, was analyzed by XRD and Scanning Electron Microscopy (SEM) to determine its phase chemistry. The K-3 REDOX was analyzed by dissolution in H_2SO_4/HF in the presence of NH_4VO_3 [27] followed by colorimetric analysis for Fe^{2+} and total Fe expressed as $\sum$Fe. The K-3 density was also measured.

The Monofrax™ K-3 brick was sectioned into coupons for corrosion testing. The K-3 coupons were taken from the center of the brick and not the "hot wall" face. The coupons were immersed in a high nitrate/nitrite oxidized feed where molar nitrate/nitrate was >> molar reductant (formate)[f] in high purity sealed Al_2O_3 crucibles. The refractory coupons stayed immersed in the feed/glass during the fusion of the feed into glass so that general corrosion rates could be measured. The crucibles were heated at 5°C per minute until a melt temperature of 1150°C was reached. Crucibles were held at 1150°C for various times, e.g. 4, 24, and 120 hours. At the end of the designated time, the crucibles were removed from the furnace and air quenched. The air quenching of the glass melt in the crucible and sectioning of the coupon imbedded in the glass allowed the mechanism by which the reaction products formed to be studied and to assess if the reaction products detach from the reaction surface.

After heat treatment, the Al_2O_3 crucibles were sectioned and a segment of the K-3 still in contact with the glass was removed and mounted in epoxy. The epoxied sample was designed to fit into the SEM. In this manner the corrosion rate of the refractory in the glass and any corrosion products formed at the Monofrax™ K-3/glass interface could be examined. K-3 was also tested in an identical fashion in pre-reacted SRNL165 glass as a control standard for comparison to the crucible studies performed by SRNL researchers in 1978-1985 time frames. This modification of ASTM C621 in sealed crucibles provides more information about the mechanisms of refractory corrosion than the ASTM C621 procedure which merely measures a dimensional loss of material.

Untreated refractory corrosion coupons made from K-3 were also immersed in the Savannah River National Laboratory (SRNL) mini-melter during operation with the DWPF nitric acid (oxidizing) flow sheet.[ξ] During this campaign there was virtually no cold cap (<10 %) based on visual observation and video films. Samples were hung half way into the glass melt pool

[f] 0.694M NO_3^- and 0.009M NO_2^- versus 0.40M $COOH^-$

[ξ] 0.616M NO_3^- and <0.002M NO_2^- versus 0.85M $COOH^-$

on platinum wires so that the corrosion depth could be measured at the melt line and in the plenum (vapor space).

4.0 RESULTS

4.1 Chemical and Phase Analysis of Monofrax™ K-3 Refractory

The composition of the Monofrax™ K-3 refractory as given by the manufacturer reports the iron content as Fe_2O_3 (Table 2). However, the manufacturer provided the following information: (1) the iron component of the Monofrax™ K-3 refractory is a mixture of predominately FeO and metallic Fe° with only small traces of Fe_2O_3, (2) the metallic iron component is used for REDOX control during the casting of the refractory to keep the oxidation state of the Cr component as +3, i.e. to promote the formation of Cr_2O_3, and (3) the Fe° component of a given refractory brick is about 0.3 volume % in the outer (hot wall face) of the refractory, 0.4% at 2.54-5.08 cm depth, 0.5% at 5.08-7.62 cm depth, 0.7% at 7.62-10.16 cm depth, 1.0% at 10.16-12.70 cm, and 1.5% at 12.70-15.24 cm depth.

Due to the variability of the Fe° content of the Monofrax™ K-3 as a function of depth in the brick, two samples of an as-received brick were analyzed for the relative concentrations of Fe^{2+} and total iron.[11] Samples were taken from near the hot wall face and in the center of the brick to ensure that the effects of the varying amounts of Fe° were accounted for. The measured REDOX ratio, expressed as $Fe^{2+}/\sum Fe$, was measured to be 0.939 (94% reduced) to 0.917 (92% reduced).[11] These results indicate that the Monofrax™ K-3 refractory is, indeed, highly reduced and that 5.4 to 5.5 wt% of the 5.9 wt% Fe_2O_3 is FeO and/or Fe° (Table 2). Determination of the FeO content of the Monofrax™ K-3 refractory provided the composition data needed to overlay the K-3 composition on Figure 1 (inset). The position of the Monofrax™ K-3 in Figure 1 serves as a reference to relate the Monofrax™ K-3 refractory composition to other known high Cr_2O_3 refractories that have been studied.[13]

To better understand the corrosion potential of the Monofrax™ K-3 refractory, especially the susceptibility to oxidizing verses reducing feeds, the chemical and phase composition of the refractory was determined. Since spinels are extremely difficult to dissolve, the bulk composition of the refractory as given by the manufacturer in Table 2 was considered to be sufficiently accurate. The "others" portion of the manufacturer's composition was evaluated by X-Ray Diffraction (XRD) and SEM/EDAX analysis. Due to the known inhomogeneity in Fe° content throughout a given Monofrax™ K-3 brick, six different samples were sent for XRD and SEM/EDAX analysis.

Analysis by XRD indicated that the Monofrax™ K-3 brick was composed of a solid solution of Al_2O_3-Cr_2O_3,[1] a magnesium aluminum chromium spinel, $MgAlCrO_4$,[2] SiO_2,[3] traces of TiO_2,[4] FeO, and metallic Fe° (Table 3). These identifications were confirmed by SEM/EDAX analysis.

[1] Powder Diffraction Files #10-173 and #38-1479
[2] Powder Diffraction Files #23-1221
[3] Powder Diffraction Files #33-1161
[4] Powder Diffraction Files #21-1276

Figure 2 shows the open porosity of the fuse cast Monofrax™ K-3 refractory. Figure 3 and Figure 4 show the presence of a rippled phase which appears to have been molten at the time that the K-3 brick was fabricated. This interstitial phase is comprised of Cr, Fe, Al, Mg and oxygen when analyzed by SEM EDAX. Thus, the interstitial phase appears to be a complex spinel solid solution of $(Fe,Mg)(Al,Cr)_2O_4$ spinel as indicated in Figure 1.

Large blocky phases, such as those in Figure 3 and Figure 4, are comprised of Cr, Al, and oxygen by SEM EDAX analyses. The large blocky phases most likely represent the Al_2O_3-Cr_2O_3 solid solution identified by XRD (Table 3). Small cubic phases in Figure 3 and Figure 4 appear to be $FeAlCrO_4$ spinel that may form a solid solution with the $MgAlCrO_4$ spinel observed by XRD. In Figure 3 another spinel, $FeCr_2O_4$ was also present as small flat globular or circular phase(s). Spheres and molten interstitial phases of predominately Fe°, in the absence of oxygen but occasionally containing some Cr° in Figure 3 and Figure 4, appear to be metallic Fe° or a solid solution of Fe°-Cr°. Several large striated grains such as that shown in Figure 5 were found and identified as metallic Fe° or an FeO-Fe° solid solution as there was little oxygen present in the SEM EDAX analyses of this phase.

Coupling the chemical analysis of Monofrax™ K-3 in Table 2 with the phase analysis in Table 3 allows the composition of the Monofrax™ K-3 refractory to be plotted on the chrome refractory ternary phase diagram in Figure 1. The density of the K-3 refractory was measured as 3.9 g/cc by measuring the weight and dimensions (length, width and height) of a complete Monofrax™ K-3 brick.

4.2 Crucible Testing of Monofrax™ K-3 Refractory in Oxidizing Feeds

The stability of the Monofrax™ K-3 refractory was tested in two melter feed batches given in Table 4. The first feed was a very oxidizing feed (nitrate of 0.69M) produced during the development of the original DWPF sludge-only flowsheet. The oxidizing feed was produced by adding prefabricated glass frit (SRNL200) to the feed product which contained 43,000 mg/L nitrate, 4000 mg/L nitrite, and 18,000 mg/L of formate. This feed was used for the crucible studies (Table 4).

Small rectangular coupons about 2.54 cm by 2.54 cm by 1.27 cm of Monofrax™ K-3 refractory were cut from a larger manufactured refractory brick. Tests were performed in sealed crucibles so the feed controlled the oxygen fugacity inside the crucible during the feed to glass conversion. The coupons were completely immersed in the feed and thus in the final glass so that general corrosion depths could be measured. The crucibles were held at 1150°C for 4, 24 and 120 hours which is 0.17, 1, and 5 days, respectively.

The coupons were sectioned making sure that the refractory sample was retrieved imbedded in the glass in order to study the mechanism by which the reaction products formed and spalled off into the glass. If the refractory/glass interface remains intact during sectioning, the reaction depths can be more accurately measured and reaction product assimilation, if any, can be studied instead of merely measuring a dimensional loss of material as is done in the ASTM 621 procedure. One sample was immersed in pre-reacted glass (DWPF reference

SRNL165 glass) as a control standard. The SRNL165 glass is the same waste glass used in the testing by previous SRNL researchers as discussed in Section 2.3.

The dual reaction layers observed by Rankin [19,21] were observed in all of the Monofrax™ K-3 coupons tested in this study. Where applicable, both measurements are given for comparison, see Table 5. It should be noted that, based on the refractory corrosion study of Cooper and Nicholson, [16] glass flow can cause the outer reaction layer to spall off exposing the penetration layer as the next reaction surface. Therefore, "average loss of material" depths may underestimate refractory corrosion in highly convective, highly stirred, or bubbled melts, while "total penetration" depths may be overly conservative in non-agitated, low-flow environments. The total penetration depths are preferentially reported in this study as being the most conservative measure of refractory wear.

The corrosion of Monofrax™ K-3 in SRNL165 glass was used as a control standard since the corrosion rate of K-3 had been measured by Corning (Table 5) using the ASTM C621 test protocol in this same glass. In this study the as-received Monofrax™ K-3 refractory was exposed to DWPF SRNL165 glass in sealed crucibles for 5 days at 1150°C. The control sample in this study gave a measured corrosion rate corresponding to an "average loss of material" of 0.79 mils/day. This value is in good agreement with the 0.68 mils/day and the 0.79 mils/day reported by Corning [25] and is in agreement with the 131 average waste glass measured corrosion rate of 0.64 mils/day [19] (see Table 5 and Table 6). Likewise, the total penetration depth measured from Figure 6 is 1.97 mils/day. Total penetration data were not reported for the SRNL165 glass testing done by Corning (Table 5). The total penetration depth of 1.97 mils/day measured in this study corresponds well with the 1.92 mils/day total penetration depth measured for 131 glass (Table 5) [19] which is of similar composition. The comparative corrosion rates for the control standards between the current study and previous studies are shaded in Table 5.

The results of corrosion measured as a function of time are given in Table 6. The corrosion mechanism is shown to be a depletion in the Al_2O_3 and MgO components of the brick (Figure 7), which leaves the corroded layer containing mostly Cr_2O_3 (Figure 7). This is in agreement with the findings of Miller and Steggs [10] discussed in Section 2.1: the Al_2O_3 phase of the Monofrax™ K-3 brick was much more vulnerable to solution in glass than the chrome (Cr_2O_3) phase. In addition, Fe_2O_3 and NiO were found to be enriched in the corrosion layers of the Monofrax™ K-3 in this study (Figure 7). The NiO is a minor component of the glass (~1 wt%). The Monofrax™ K-3 contains no NiO but was shown in this study to react with NiO from the glass forming a Ni-Fe-Cr rich spinel reaction product.

The Fe_2O_3 enrichment seen in Figure 7 is likely coming from the glass although there is Fe_2O_3 in the Monofrax™ K-3 refractory. The enrichment of the corroded layer in Fe over the amount of Fe in the bulk refractory suggests that iron oxide from the melt is absorbed by the refractory as observed by Maun and Osborn [13] in other chrome refractories and by the K-3 manufacturer [10]. Since the Fe_2O_3 is ~12 wt% of the glass melt, the melt could become enriched in other glass constituents such as SiO_2 in the region closest to the refractory causing local increases in glass viscosity in the refractory contact zone.[28] Increases in Al_2O_3 dissolved from the refractory can also cause a local increase in the glass viscosity in the refractory contact zone. Silicon appears slightly depleted in the corrosion layers (Figure

7) but since the concentration of SiO_2 is so low in the refractory this amount would have little impact on the glass or the glass viscosity near the refractory contact zone. Analysis of Figure 7 confirms that the Monofrax™ K-3 corrosion in DWPF type glasses is a strong function of the nickel oxide and iron oxide content of the glass: Ni and Fe in the glass exchange for Mg and Al in the refractory. [10]

Figure 8 shows the growth of crystalline K-3 corrosion products. The crystalline masses protrude from the interface between the corrosion front and the penetration front like blisters (SEM in Figure 8). These blisters clearly volume expand as expressed by Muan and Osborn [13] as a "bursting expansion." While the bursting expansion had been described for Cr_2O_3 refractories Figure 8 is the first micrograph of the phenomena.

The bulk Monofrax™ K-3 is rich in Al and Cr (region #1 in Figure 8). The area between the penetration front and the corrosion front (region #2) is defined by the row of protrusions or "tufts" of crystallized material. While region #2 is still rich in Al and Cr, species such as Mn, Ni, and Fe are diffusing into the refractory from the glass as they comprise major components of this region (Figure 8). The region between the corrosion front and the outside of the sample (region #3) becomes progressively more enriched in Cr and Fe while becoming depleted in Mg and Al toward the outside surface of the sample (region #4 in Figure 8) until there is no refractory matrix left to hold the Cr and Fe rich "reaction layer" (region #5 in Figure 8). At this point the Fe-Cr-Ni rich "crust" spalls off into the glass melt as $Ni(Cr,Fe)_2O_4$ spinel (see detached inclusions in region #5 and region #6 in Figure 8). Figure 9 provides an enlargement of the $Ni(Cr,Fe)_2O_4$ spinel, which is insoluble in the melt, spalling off into the bulk glass where it may continue to adhere to the melter wall or fall to the bottom of the melter depending on melt agitation.

The depletion of the refractory in Mg is likely responsible for the formation of the refractory corrosion product, krinovite ($NaMg_2CrSi_3O_{10}$) found in the deposits of the IDMS melter floor [29]. The decomposition of high chrome-alumina refractories into magnesium silicates and $MgO{\bullet}Cr_2O_3$ is predicted by the known phase equilibria in the $MgO\text{-}Cr_2O_3\text{-}SiO_2$ system [13] that has been used to monitor degradation of chrome-alumina refractories in the steel industry [13].

4.3 Pilot Scale Melter Testing of Monofrax™ K-3 in Oxidizing Feed

Validation of the corrosion rates measured in crucibles was provided by the $1/100^{th}$ DWPF mini-melter experiments. As received K-3 coupons were immersed in the mini-melter while testing current DWPF oxidizing flow sheet with 0.62 molar nitrate, 0.85M formate, and SRNL200 frit feeds (Table 4). Other than the differences in nitrate and formate content of this feed compared to the feed used in the crucible studies, both feeds had similar amounts of waste and frit, similar sulfate content, and converted to glasses with approximately the same concentration of Na_2O, i.e. 12.7 wt% and 12.2 wt% (Table 4).

Coupons of Monofrax™ K-3 were immersed in the mini-melter melt pool and partly exposed in the melter plenum vapor space. The measured penetration depth for the Monofrax™ K-3 at approximately the melt line was 7.87 mils or a rate of 2.62 mils/day (Table 5) and 2.36 mils in the melt region or a rate of 0.79 mils/day (Table 5). The corrosion rate measured in

the 3-day mini-melter test is 2.62 mils/day compared to the 5-day crucible test results shown in Table 5 which gave 2.49 mil/day in oxidizing feeds.

The dual corrosion zones identified in the crucible studies were also observed in the 1/100th scale mini-melter refractory coupon tests. The $Ni(Cr,Fe)_2O_4$ spinel enriched reaction layer can also be seen in Figure 10 and the spinel corrosion products can be seen spalling off into the attached glass for both the melt line and vapor space parts of the coupon. The same depletion of Al and Mg seen in the crucible tests were seen in the mini-melter refractory coupon tests.

It was difficult to tell exactly where the melt line was on the refractory coupon immersed in the mini-melter due to splatter from the melt pool (there was <10% cold cap coverage during all of the campaigns). However, measurements on this coupon in the vicinity of the melt line indicated that the ratio of the two corrosion depths, i.e. the "average loss of material"/"total penetration," was the highest of any of the K-3 coupons tested in this study (Table 5), i.e. the outer corrosion layer was the largest fraction of the total penetration depth. The top of this same Monofrax™ K-3 coupon had been exposed to the mini-melter vapor space and exhibited a lower "average loss of material"/"total penetration" ratio (Table 5 and Figure 10). Note in Figure 10 that the same spalling of the $Ni(Fe,Cr)_2O_4$ spinel corrosion products is observed as in the sealed crucible studies during the feed to glass conversion.

5.0 DISCUSSION: ACCELERATED CORROSION MECHANISMS

5.1 Accelerated Corrosion Mechanisms for Monofrax™ K-3 Refractory

The data given in Table 5 are for varying total test durations of Monofrax™ K-3 coupons to pre-reacted molten glass or feed. To compare the relative corrosion rates, the corrosion depth (mils) measured is normalized by dividing by the test duration (days), e.g. mils/day. This normalization also allows some preliminary comparisons of the relative corrosion rates measured in crucible tests to be compared to the rates observed in the SRNL mini-melters over longer periods of time, e.g. 1 and 2 years of continuous operation. However, the measurement of mils/day corroded is an asymptotic function of test duration. Therefore, corrosion testing should be carried out for a variety of time durations and plotted linearly as total mils corroded versus time as done in Figure 11. This provides linear rate equations expressed as $\partial d/\partial t$, where d is depth in mils and t is time in hours.

In this study, the corrosion of the Monofrax™ K-3 was measured (in triplicate) for three different time periods, e.g. 4, 24, and 120 hours. The 120-hour or 5-day coupon test results are those given previously in Table 5 as mils/day and expressed in Table 6 as depth of attack ("total penetration") and depth of the outer "average loss of material" layer in mils. The linearity of the K-3 corrosion as a function of time is shown in Figure 11 and the observation that the corrosion products spall off into the surrounding glass in semi-static crucible studies indicates that a protective or passivation layer may not be forming on the K-3 refractory when the melter is processing highly oxidizing feeds.

The data in Table 6 give the following linear corrosion rates (Figure 11):

$$\text{Corrosion (mils)}_{\text{K-3 total penetration}} = 3.040 + 1.88 \text{ time (days)} \quad R^2=0.83 \quad (1)$$

$$\text{Corrosion (mils)}_{\text{K-3 loss of material}} = 1.225 + 1.34 \text{ time (days)} \quad R^2=0.97 \quad (2)$$

Note that the "average loss of material" measurement is more accurate than the "total penetration depths" as the average loss is easier to measure on the micrographs.

The relative rates, as indicated by Equations 1 and 2 give linear corrosion rates of 4.92 mils/day for total penetration and 2.57 mils/day for loss of material. The latter 2.57 mils/day for loss of material is in agreement with the average of the triplicate crucible study values given in Table 5 of 2.49 mils/day. Thus the loss of material is slower than the total penetration rates. This result is also suggested in Table 6 where the measured depth for the loss of material was the same for all three replicate samples indicating that a steady state may be achieved at times >5 days in contact with glass or feed.

Measuring the total corrosion as a function of the thickness of both of the outer and inner reaction zones indicates that the corrosion rates measured in oxidized feeds were 1.8-2.8 times greater than those measured previously (Table 5). However, the measured corrosion rates in oxidized feeds shown in Table 5 for the crucible studies and mini-melter tests described in this study were still less than the 3, 5.4 and 7.5 mils/day allowable DWPF Design Basis [1] for the melter bottom, sidewall, and melt line.

The data presented above on the corrosion of the Monofrax™ K-3 in highly oxidized DWPF feeds suggest that the presence of feed additives, high nitrate oxidizing feed/melt conditions, the highly reduced Monofrax™ K-3 is thermodynamically unstable (Equation 3 below). The oxidizing conditions destabilize the reduced Fe^{2+} and Fe° and possibly Cr^{3+} species in the Monofrax™ K-3 brick which accelerates the Monofrax™ K-3 corrosion.

By knowing the approximate composition of the K-3 corrosion products from a post melt mini-melter analysis, it can be shown from thermodynamic calculations that the $Ni(Cr_{0.8}Fe_{0.2})_2O_4$ spinel Monofrax™ K-3 corrosion product that forms in oxidized melts is thermodynamically more stable at a melt temperature of ~1150°C than the $MgAlCrO_4$ spinel composing the bulk of the K-3 refractory. Using thermodynamic data from Barin [30] at 1400°K (~1130°C) and writing a partial reaction for Fe_2O_3, NiO, and SiO_2 in a glass reacting with $MgAlCrO_4$, the major spinel phase in the K-3 refractory, to form a $NiCrFeO_4$ spinel reaction product, plus $MgO{\bullet}SiO_2$ (proto-enstatite),[ξ] SiO_2 (cristobalite) or $Al_6Si_2O_{13}$ (mullite) [13] yields Equation 3.

Writing similar partial reaction for the reaction of the reduced iron-containing spinels in the Monofrax™ K-3 (minor refractory components) and FeO (minor component) in the K-3 refractory, reacting with NiO and SiO_2 and O_2, where the O_2 is released by the denitration of the oxidized feeds, in the melt to form the same $NiCrFeO_4$ spinel and mullite yields Equation

ξ $MgO{\bullet}SiO_2$ and SiO_2 or mullite reaction products and $MgO{\bullet}Cr_2O_3$ from the refractory further react with Na_2O in the glass to form the silicates like Krinovite, ($NaMg_2CrSi_3O_{10}$).

4. These reactions indicate that the decomposition of the K-3 into $NiCrFeO_4$ spinel and silicates is favored in high transition metal waste glass melts at temperatures of ~1150°C. Equation 4, which contains the impact of the oxidizing feeds, is favored over Equation 3 which is written without the O_2 from denitration reactions.

$$\underbrace{6MgAlCrO_4}_{Major\ K-3\ phase} + \underbrace{3Fe_2O_3 + 6NiO + 8SiO_2}_{melt} \rightarrow \underbrace{6NiCrFeO_4 + 6MgO \bullet SiO_2 + Al_6Si_2O_{13}}_{observed\ and\ predicted\ chrome\ refractory\ products} \quad (3)$$

$$\Delta G_{fm}(products) - \Delta G_{fm}(reactants) = -1759\ KJ / mole$$

$$\underbrace{6FeAlCrO_4 + 2FeCr_2O_4 + 2FeO}_{K-3\ phases} + \underbrace{10NiO + 2SiO_2 + 2.5O_2}_{melt} \rightarrow \underbrace{10NiCrFeO_4 + Al_6Si_2O_{13}}_{observed\ and\ predicted\ chrome\ refractory\ products} \quad (4)$$

$$\Delta G_{fm}(products) - \Delta G_{fm}(reactants) = -3128\ KJ / mole$$

In this study it has been shown that the Cr enriched $NiFe_2O_4$ spinels that form as refractory corrosion products can fall or spall off into the waste glass. It is predicted that these Cr enriched spinels can agglomerate in the melt pool [31,32] and ultimately accumulate on the floor of a melter and/or periodically become entrapped in the riser or pour spout [31] although no accumulations have been seen in pour spout samples taken from the DWPF over the last 20 years.[33]

The enhanced corrosion at the melt line shown in the average loss of material (mils/day) in Table 5 is believed to be the combined effect of mechanisms such as those given in Equations 3 and 4 and also from interaction with the oxidizers, mainly nitrates in the feed which are reacting in the cold cap to release O_2 and N_2. [48]

The addition of oxidizers to the melter feed vessels can chemically oxidize transition metal species to higher valence states than the equilibrium valence states of these species entering from the waste tanks. An assessment can be made of the degree to which nitrate species entering the melter drive the oxidation of these species by examining the REDOX half reactions (Table 7 Equations 5 to 11). The oxidation reactions, if they occur in the melter or cold cap, can oxidize transition metal species in the reduced refractory at or near the melt line. The E° for the REDOX half reactions is proportional to the free energy, ΔF, for a given reaction. Although values for E° are normally based in aqueous environments, it is assumed in this discussion that the E° for the half reactions in the cold cap or molten glass environment would reflect the thermodynamic "driving force" and are be used to estimate the relative effects of different chemical reactions.

From the Table 7 half reactions (Equations 6 and 11), it can be seen that the oxidation potential of nitrate to N_2 will "drive" Fe^{2+} to Fe^{3+} (Equation 12 below gives the full reaction). This prediction is confirmed by the very oxidized $Fe^{2+}/\sum Fe$ ratios of the glasses poured during the 1.75 year non-radioactive DWPF campaigns, where the concentration of the Fe^{2+}

was less than the analytic detection limit; i.e.; almost all of the Fe^{2+} had been oxidized to Fe^{3+} under these melt conditions.

The combined E° for the overall nitrate to N_2 reaction (Equation 6) and Fe^{+2} to Fe^{+3} reactions (Equation 11) given in Table 7 are additive, i.e. $E = E°_1 = E°_2$. Therefore,

$$E° = E° (\text{for } NO_3^- \text{ to } N_2) - E°(\text{for } Fe^{+2} \text{ to } Fe^{+3})$$
$$= (+1.24) + (-0.77) = +0.57 \text{ volts} \quad (12)$$

And here the convention is that a positive potential in volts is a spontaneous reaction. [34] So any Fe^{+2} in the refractory can be oxidized by the nitrate going to N_2 (Equation 6).

For Cr^{+3} in the refractory (Equation 7 in Table 7) when coupled with Equation 6 (in Table 7) for nitrate going to N_2, the reaction is not favored (negative potential).

$$E° = E° (\text{for } NO_3^- \text{ to } N_2) - E°(\text{for } Cr^{+3} \text{ to } Cr^{+6})$$
$$= (+1.24) + (-1.33) = -0.09 \text{ volts} \quad (13)$$

Therefore, the Cr^{+3} in the refractory stays as Cr^{+3} in the $Ni(Cr_{0.8}Fe_{0.2})_2O_4$ corrosion products of the K-3.

While manganese is not in the K-3 refractory, it is present in the feed as Mn^{+2} which can also spontaneously oxidize to Mn^{+4} (Equations 6 and 8 in Table 7) in the presence of nitrate in the cold cap

$$E° = E° (\text{for } NO_3^- \text{ to } N_2) - E°(\text{for } Mn^{+2} \text{ to } Mn^{+4})$$
$$= (+1.24) + (-1.21) = +0.03 \text{ volts} \quad (13)$$

However, if manganese is present in the feed as Mn^{+4} it can only oxidize spontaneously to Mn^{+7} if nitrite goes to N_2 (Equations 5 and 9 in Table 7) as Equations 6 and 9 would yield a negative potential and not be favored.

$$E° = E° (\text{for } NO_2^- \text{ to } N_2) - E°(\text{for } Mn^{+4} \text{ to } Mn^{+7})$$
$$= (+1.77) + (-1.68) = +0.09 \text{ volts} \quad (14)$$

This was recently observed during REDOX modeling of Mn species in the presence of nitrate and nitrite.[35]

Therefore, the oxidized melt degrades the Monofrax™ K-3 wherever the melt comes in contact with the refractory by reactions such as those given in Equations 5 and 6 (Table 7). There is a reduced driving force for these reactions with a more reduced melt. Therefore, it is the oxidation of the refractory from nitrates and nitrites that is likely responsible for the enhanced degradation rates observed at the melt line.

6.0 CONCLUSIONS

The K-3 corrosion was determined to be incongruent or heterogeneous in all feeds tested including those of the commercial fiberglass industry. As determined by previous researchers, the Monofrax™ K-3 refractory surface becomes depleted in Al_2O_3, MgO, and Cr_2O_3 leaving a porous outer corrosion layer that allows reaction with Fe_2O_3 and NiO from the waste glass. Glasses with higher Na_2O content appear to solubilize the Al_2O_3 component of the Monofrax™ K-3 more rapidly. Although the Monofrax™ K-3 brick does not contain NiO, its primary corrosion reaction product is $Ni(Cr,Fe)_2O_4$ spinel. Free energy and REDOX potential calculations indicate that the DWPF high nitrate oxidizing feed and melt conditions likely act as driving forces for attack by oxidative dissolution of the highly reduced Monofrax™ K-3, i.e. the Monofrax™ K-3 is unstable in highly oxidized feeds based upon these computations.

Measuring the total corrosion as a function of the thickness of both of the outer and inner reaction zones indicated that the corrosion rates measured in oxidized DWPF feeds were approximately 1.8-2.8 times greater than those measured previously. However, the measured corrosion rates, even in oxidized feeds, were less than the 3 mil/day allowable DWPF Design Basis. The corrosion tests with the oxidizing feed also indicated that the measured corrosion rates were higher than those measured with either pre-reacted glass (ASTM C621) or more reducing feeds in large pilot scale testing at SRS.
Mechanistically, two different reaction (corrosion) layers were observed to form on the Monofrax™ K-3 surface during the feed to glass conversion as observed in previous tests with pre-reacted glass (ASTM C621):

- an outer layer of poorly attached reaction products designated by previous researchers as the region of "average loss of material" and
- an inner reaction designated by previous researchers as the region of "total penetration."

The K-3 corrosion rates from the crucible tests were shown to be approximately linear as a function of time (4 hours, 24 hours, and 120 hours) in DWPF oxidizing feeds. In addition, K-3 coupons had been immersed at the glass melt line and in the vapor space in the SRNL mini-melter for 3 days. The mini-melter was processing DWPF oxidizing feed at the time of the corrosion coupon testing.

The specific conclusions based on the studies performed indicate that oxidizing melter flowsheets can contribute or cause the following:

- accelerated Monofrax™ K-3 refractory degradation relative to previous testing in pre-reacted glass by ASTM C621
  - Monofrax™ K-3 was analyzed to be 92-94% reduced as measured by its $Fe^{+2}/\sum Fe$ ratio
  - corrosion testing of Monofrax™ K-3 in crucibles in oxidized feeds gave measured corrosion rates that were ~1.8-2.8 times higher than the rates measured in pre-reacted glass by previous researchers

- corrosion testing of the Monofrax™ K-3 in the SRNL minimelter in oxidizing DWPF feeds gave similar corrosion rates to those measured in oxidized feed crucible tests
- corrosion testing in pre-reacted 165 glass in this study was comparable to measurements with this same glass in previous studies
- the corrosion mechanism in the 165 glass was shown to be by attack of the Al_2O_3 component of Monofrax™ K-3 by Na_2O, NiO, and Fe_2O_3 in the oxidized glass
- free energy calculations demonstrated that the accelerated corrosion mechanism in the DWPF oxidized feeds is likely oxidative dissolution of the reduced transition metals present in the Monofrax™ K-3
- calculation of REDOX potentials for the various REDOX half reactions demonstrated that NO_3 can oxidize reduced iron species in the refractory but not the chromium species. However, the chromium species in the refractory can be oxidized by nitrite.
- the REDOX potentials also indicate that nitrate can oxidize Mn^{+2} to Mn^{+4} but only nitrite species can oxidize Mn^{+4} to Mn^{+7} in the feed.

• gas-glass disequilibrium
  - gas-glass disequilibrium causes bubble formation; bubble formation impacts Monofrax™ K-3 refractory corrosion by rapidly replacing refractory-saturated glass, which can act as a protective layer, with fresh glass causing accelerated Monofrax™ K-3 corrosion

The spinel products formed from the degradation of the Monofrax™ K-3 refractory do not sequester any radionuclides other than Ni^{59} and Ni^{63} and Fe^{55}. However, the Ni radioisotopes are 3 orders of magnitude lower than non-radioactive Ni and Fe^{55} has decayed away since the waste was generated. The non-radioacitve Ni in the waste is derived from the dissolution of Ni cladding from fuel rods and the non-radioactive Fe in the waste is derived from the use of ferrous sulfamate in the Purex process, these concentrations are far in excess of their radioactive isotopes. Moreover, the slag on the melter floor and walls is an average of ~35 wt% spinel and ~65 wt% waste glass.[1] The amount of radioactivity in the glass portion of the slag will be greater than that in the spinel corrosion products from the Monofrax ™ K-3 refractory. Defense waste glass melters at the SRS have lasted 9 and >11 years respectively [1,36] and failed melters are drained of glass and stored in special vaults in the vitrification facility for decommissioning at the end of the facility life.[37]

7.0 ACKNOWLEDGMENTS

The authors would like to gratefully acknowledge the assistance of SRNL's Analytic Development personnel. This paper was prepared in connection with work done under Contract Nos. DE-AC09-76SR00001, DE-AC09-96SR18500, DE-AC09-08SR22470 with the U.S. Department of Energy.

APPENDIX A. Solubility and Redox Equilibria of Cr_2O_3 in Glass

Chromium oxide has poor solubility in borosilicate glass (~0.30 wt% Cr_2O_3) [38] and in other types of glass (0.5-2.0 wt%) [39]. If the solubility of Cr^{+3} as Cr_2O_3 is exceeded, discrete particles (black "dots") of Cr_2O_3 form in the bulk melt [40]. The solubility of Cr_2O_3 in glass decreases with decreasing temperature [40]. Spinel formation can also occur when the Cr_2O_3 solubility limit of a waste glass enriched in other transition metal oxides, i.e. Fe_2O_3, is exceeded. [41,42] Bates [43] observed an increase in viscosity due to crystallinity (chrome spinel formation) with increased Cr_2O_3 content in a borosilicate waste glass. Settling of chromium rich spinel has been observed in Joule-heated melters and in laboratory melts with Hanford waste glasses [44].

Thermodynamic calculations performed by Degterov and Pelton [8] indicate that the solubility limit of Cr_2O_3 from Cr_2O_3- Al_2O_3 refractories such as Monofrax K-3 is strongly dependent on the oxygen partial pressure in a melter. Although the example given by these authors is for reduced oxygen partial pressures and the Cr^{+2}/Cr^{+3} equilibria, similar[5] oxygen partial pressure dependency governs the Cr^{+3}/Cr^{+6} equilibria under oxidizing conditions [45].

According to the data of Sussmilch and Jouan [46], when the REDOX equilibrium of Cr^{+6}/Cr^{+3} in a glass melt is oxidizing, i.e. reaches the value of 0.01 or 1% Cr^{+6} and 99% Cr^{+3} corresponding [45] to an effective $pO_2=10^{-2}$ atm. or $Fe^{+2}/\sum Fe=0.04$ which is the approximate DWPF detection limit at 1150°C, then alkali chromates (Cr^{+6}) may separate from the melt concentrating as a yellow surface layer on the melt along with other alkali salts (halides, sulfates, etc.). These alkali chromates and salts are relatively soluble in water, and their presence leads to poor glass durability. Temperature also has a significant effect on the Cr^{+6}/Cr^{+3} equilibrium in a glass. Higher temperatures favor Cr^{+3} causing Cr^{+6} to reduce liberating oxygen [40]. Under reducing conditions, e.g. $Fe^{+2}/\sum Fe>0.5$ ($pO_2=10^{-8}$ atm), about 3% Cr^{+2} may also be present in a glass [40,45] at 1150°C. Between pO_2 of 10^{-2} and 10^{-8} atmospheres, Cr^{+3} is the predominant stable chromium species at 1150°C [45].

[5] Free limited access to the F*A*C*T (Facility for the Analysis of Chemical Thermodynamics) thermodynamic software used by these authors is available on the World Wide Web and model calculations involving Cr^{+3}/Cr^{+6} equilibria and its oxygen dependency were performed

Table 1. Comparison of the Concentrations of Oxidizers in HLW, LAW and LLMW at Savannah River, West Valley, and Hanford

Description	Molar NO_3^- Concentrations	Molar NO_2^- Concentrations
SRS M-Area LLMW Sludge[a]	0.68	---
SRS HLW DWPF	~0.40-0.69	---
Hanford LAW Salt Supernate[b]	3.2	1.7
Hanford HLW[c]	0.18(max)	calculated as total NO_3^-
West Valley HLW	2.4	---

[a] J.B. Pickett, Vendor Treatment Specification X-SPP-M00001

[b] WHC-SD-ER-498, Rev. O,

[c] TWRS Privatization Contract No. DE-RP06-96RL13308

Table 2. Monofrax™ K-3 Composition as Given By the Vendor and as Partially Analyzed by SRNL (see Reference 11)

Component	Carborundum Analysis (Wt%)	Component	SRNL Partial Analysis [11]
Al_2O_3	58.6	Al_2O_3	--
Cr_2O_3	27.1	Cr_2O_3	--
MgO	6.1	MgO	--
SiO_2	1.6	SiO_2	--
Fe_2O_3	5.9	Fe_2O_3	0.4-0.5 wt%
FeO	reported as Fe_2O_3	FeO	5.4-5.5 wt%
Na_2O	0.3	Na_2O	--
Other	0.4	Other	--
TiO_2	not given	TiO_2	~0.5 wt% by XRD
ZrO_2	not given	ZrO_2	trace by SEM

Table 3. Monofrax™ K-3 Phase Composition

Phase	X-Ray Diffraction (XRD)	Scanning Electron Microscopy/ Energy Dispersive Analysis by X-ray (SEM/EDAX)	Visual Characteristics
$MgCr_2O_4$-$FeCr_2O_4$-$MgAl_2O_4$-$FeAl_2O_4$[t]	--	Major	Once molten interstitial phase
Al_2O_3•Cr_2O_3	Major	Major	Large/Blocky Crystals
$MgAlCrO_4$ Spinel	Major	Major	Once molten interstitial phase
$FeCr_2O_4$	--	Minor	Large striated crystals and small flat globs
$FeAlCrO_4$	--	Minor	Small cubic crystals
Fe°	Trace	Minor	Spheres
Fe°-Cr° solid solution	---	Minor	Intergranular semi-continuous Phase
FeO	Trace	Minor	Large striated crystals
SiO_2	Minor	--	--
TiO_2	Trace	--	--
ZrO_2	--	Trace	Large cubic crystals

t these are all spinel phases which can also be written as (MgO•Cr_2O_3)-(FeO•Cr_2O_3)-(MgO•Al_2O_3)-(FeO•Al_2O_3)

Table 4. Feed Compositions Used in Monofrax K-3 Crucible and Mini-melter Tests.

Feed Constituent	Feed Used in Crucible Studies	Feed Used in Mini-melter Studies - SME Product 2-11	Units
HLW* sludge simulant Waste Loading	24.8	25.6	wt% dry oxide basis
SRNL200 frit	75.2	74.4	wt% dry oxide basis
Nitrate	0.694	0.616	Molar
Nitrite	0.0086	<0.002	Molar
Formate	0.40	0.853	Molar
Sulfate	1.69×10^{-3}	1.28×10^{-3}	Molar
Chloride	$<2.82 \times 10^{-3}$	$<2.82 \times 10^{-3}$	Molar
Fluoride	$<5.26 \times 10^{-3}$	$<5.26 \times 10^{-3}$	Molar
Melter feed solids	41	45.61	Wt %
Na_2O in Glass	12.7	12.2	Wt %
Fe_2O_3 in Glass	12.5		Wt %
Al_2O_3 in Glass	4.3		Wt %
NiO in Glass	0.07		Wt %
MnO in Glass	1.2		Wt %

*(based on waste Tank 51 composition at the Savannah River Site)

Table 5. Comparison of Monofrax™ K-3 Corrosion Depths in This Study Compared Previous SRNL ASTM C621 Measurements

Type of Measurement	Temp (°C)	Time (Days)	SRNL Frit Designations	SRNL Simulated Waste Type or Glass	Average Loss of Material (mils/day) normalized to test duration	Total Penetration (mils/day) normalized to test duration	Ratio of Loss/ Penetration	Na_2O in Waste Glass (Wt%)	Ref.
Crucible Melt Line ASTM 621	1150	7	131	Average Waste Glass from Savannah River Technical Data Summary	0.64[t]	1.92[t]	0.333	12.6	19
Crucible Melt Line* ASTM 621	1150	7	165	SRNL165 Glass	0.73[t]	ND	ND	11.0	25
Crucible Melt Line* ASTM 621	1150	7	165		0.23	ND	ND	11.0	25
Crucible Melt Line** ASTM 621	1150	7	165		0.68[t]	ND	ND	11.0	25
Crucible – Sample Immersed in Glass	1150	5	165	SRNL165 Glass	0.79[t]	1.97[t]	0.40	11.0	This study
Crucible – Sample Immersed in Feed (3 samples)	1150	5	200	High Nitrate Feed (see Table 4)	Average of 1.57	Average of 2.49	Average of 0.63	12.7	This study
Mini-melter Melt Line†	1150	3	200	Lower Nitrate Feed (see Table 4)	2.29	2.62	0.87	12.2	This study
Mini-melter Vapor Space†	1150	3	200		0.52	0.79	0.65	12.2	This study

*As cast K-3 surface; **Ground K-3 surface; †Diamond cut K-3 surface, CELS = Corning Engineering Laboratory Services, Corning, NY

t The comparative corrosion rates for the control standards are shaded.

Table 6. Corrosion Measured in K-3 Refractory Replicates in Oxidized Feeds at 1150°C

	4 HOURS	24 HOURS	120 HOURS
Reaction Layer	mils	mils	mils
Total Penetration	3.94	5.51	11.81
	3.94	5.9	15.75
	2.36	3.15	9.84
Average Loss of Material	0.985	3.15	7.88
	1.18	3.35	7.88
	1.38	2.17	7.88

Table 7. Reduction/Oxidation Half Reactions

Pertinent "Half" Reactions [47]	E° Potential, (Volts)	Equation Number
REDUCTIONS		
$N_2O + 2H^+ + 2e^- \rightarrow N_2 + H_2O$	+1.77	(5)
$NO_3^- + 6H^+ + 5e^- \rightarrow 0.5N_2 + 3H_2O$	+1.24*	(6)
OXIDATIONS		
$2Cr^{+3} + 7H_2O \rightarrow Cr^{+6}{}_2O_7^{-2} + 14\ H^+ + 6e^-$	-1.33	(7)
$Mn^{+2} + 2H_2O \rightarrow Mn^{+4}O_2 + 4H^+ + 2e^-$	-1.21	(8)
$Mn^{+4}O_2 + 2H_2O \rightarrow Mn^{+7}O_4^- + 4H^+ + 3e^-$	-1.68	(9)
$Ni^{+2} + 2H_2O \rightarrow Ni^{+4}O_2 + 4H^+ + 2e^-$	-1.93	(10)
$Fe^{+2} \rightarrow Fe^{+3} + e^-$	-0.77	(11)

*Preferred cold cap reaction for nitrate going to N_2 from Choi [48]

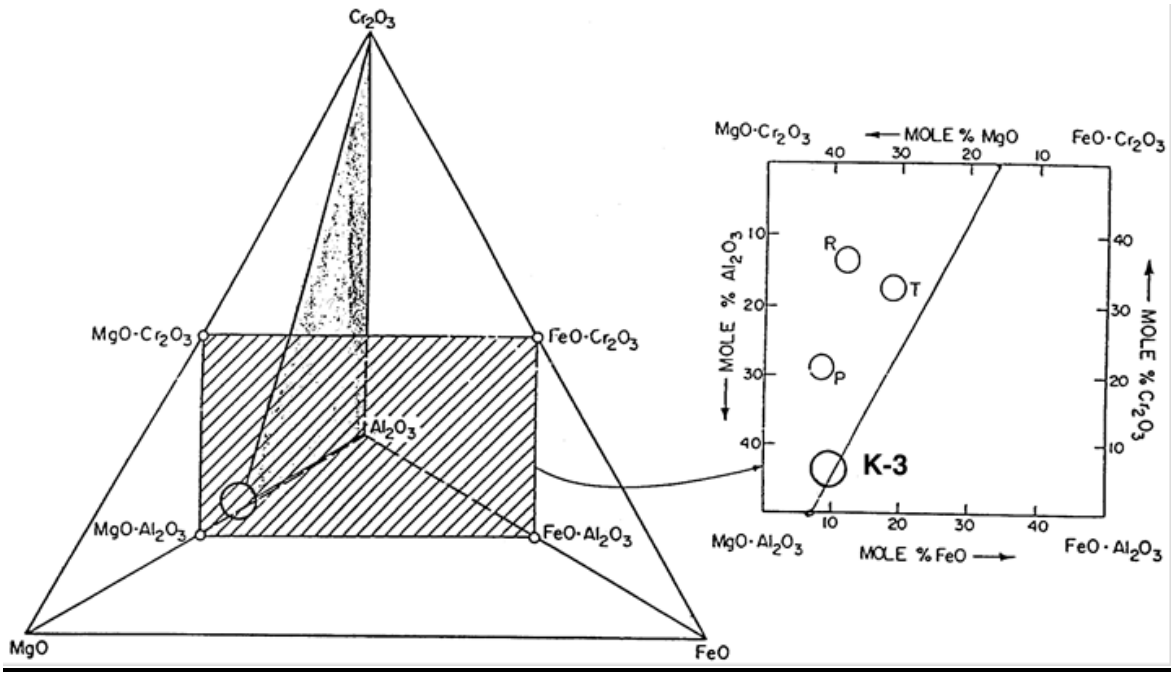

Figure 1 Tetrahedron representing the system MgO-FeO-Al_2O_3-Cr_2O_3, showing position of the solid solutions (striped region) formed during the manufacture of chrome rich refractories. The chrome ores used in the manufacture of chrome refractories also lie on this composition plane. The chrome ores recalculated to 100% of MgO, FeO, Al_2O_3, and Cr_2O_3 are plotted on a mole% basis in the upper right-hand inset sketch, where average analyses are plotted of Phillippine (P), Transvaal (T), and Rhodesian (R) ores (from Reference 13). The composition of the DWPF K-3 refractory spinel was calculated from the data in Table VI on a similar basis and overlain in the inset for comparison. The composition of the DWPF K-3 refractory, therefore, lies in a three phase compatibility triangle formed by connecting the spinel composition to the Al_2O_3 and Cr_2O_3 apices this quaternary system.

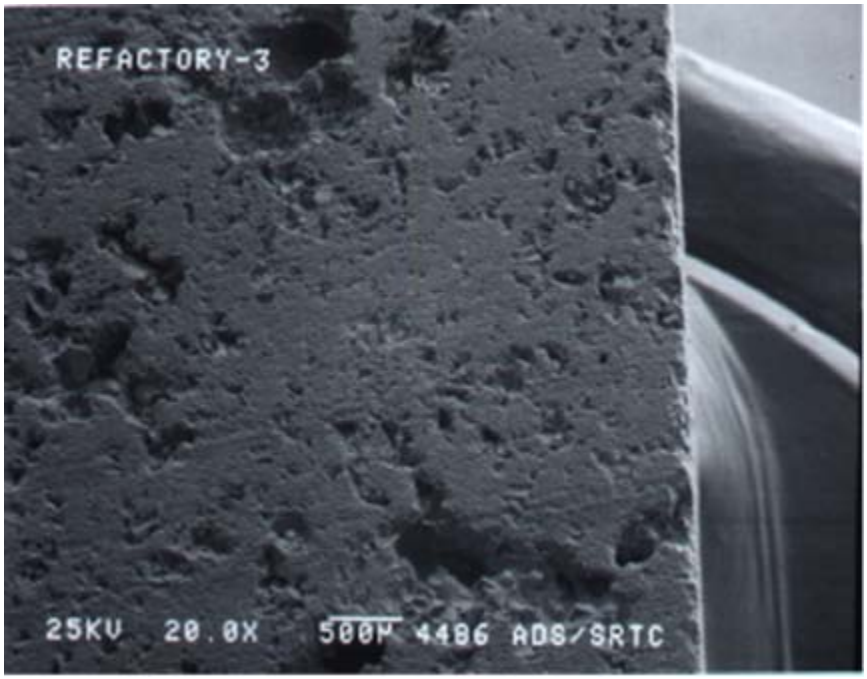

Figure 2 Scanning Electron Micrograph showing the open porosity of the K-3 fusion cast refractory.

Figure 3. Phase morphology and composition of K-3 refractory.

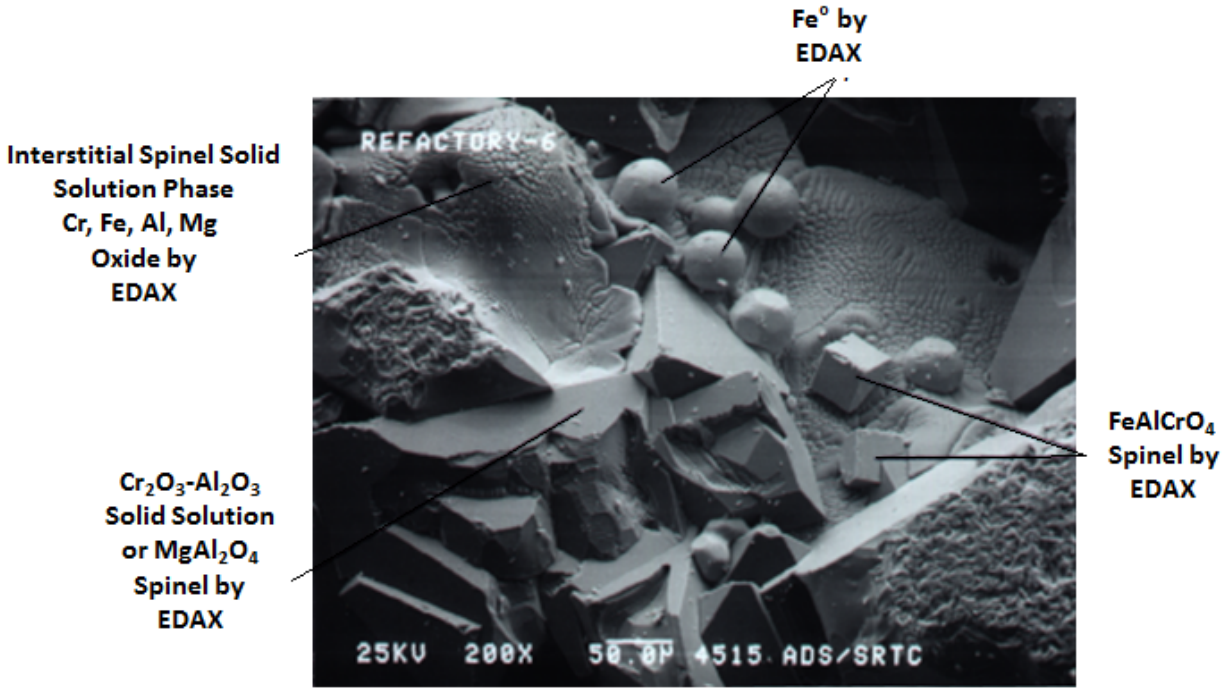

Figure 4 Phase morphology and composition of K-3 refractory.

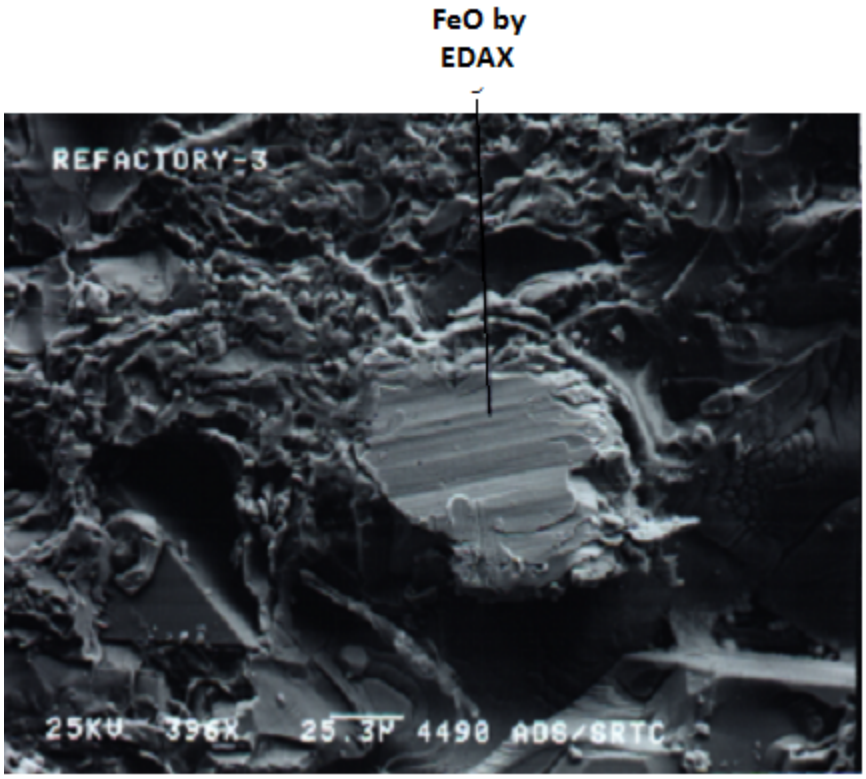

Figure 5 Phase morphology and composition of K-3 refractory.

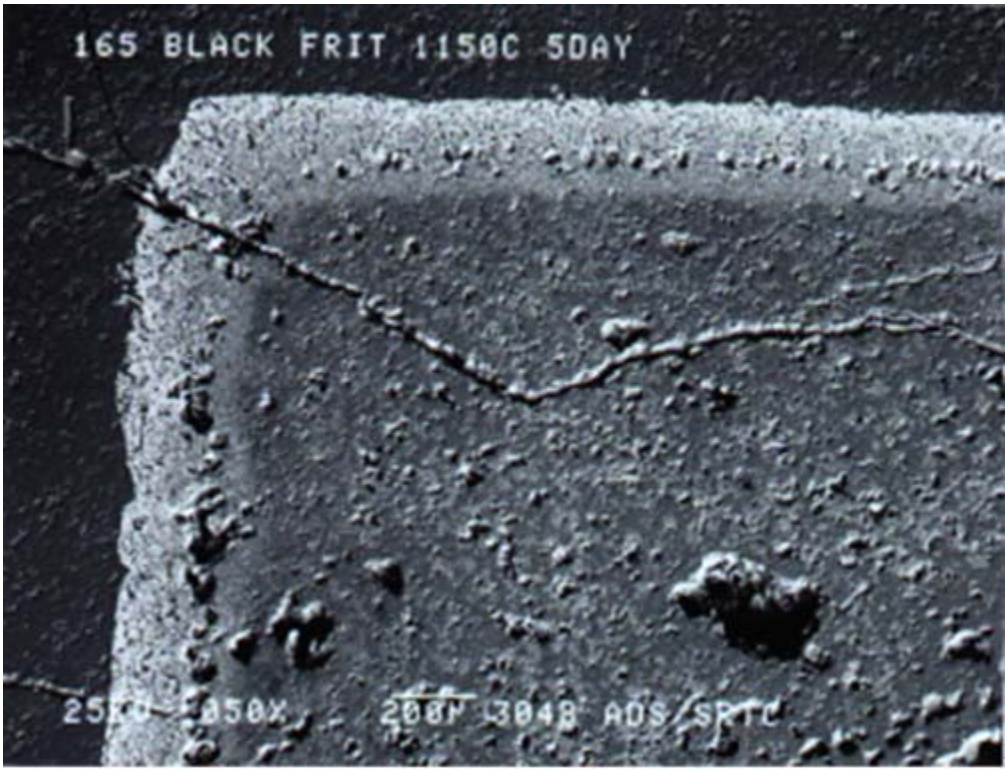

Figure 6 Scanning Electron Micrograph of the K-3 refractory corrosion coupon immersed in glass composed of SRNL165 glass for 5 days at 1150°C. Note the thick corrosion layer which is composed of two layers separated by a row of circular bubble-like precipitates. The outer layer is more porous and is designated the corrosion layer. The inner layer is termed the penetration layer.

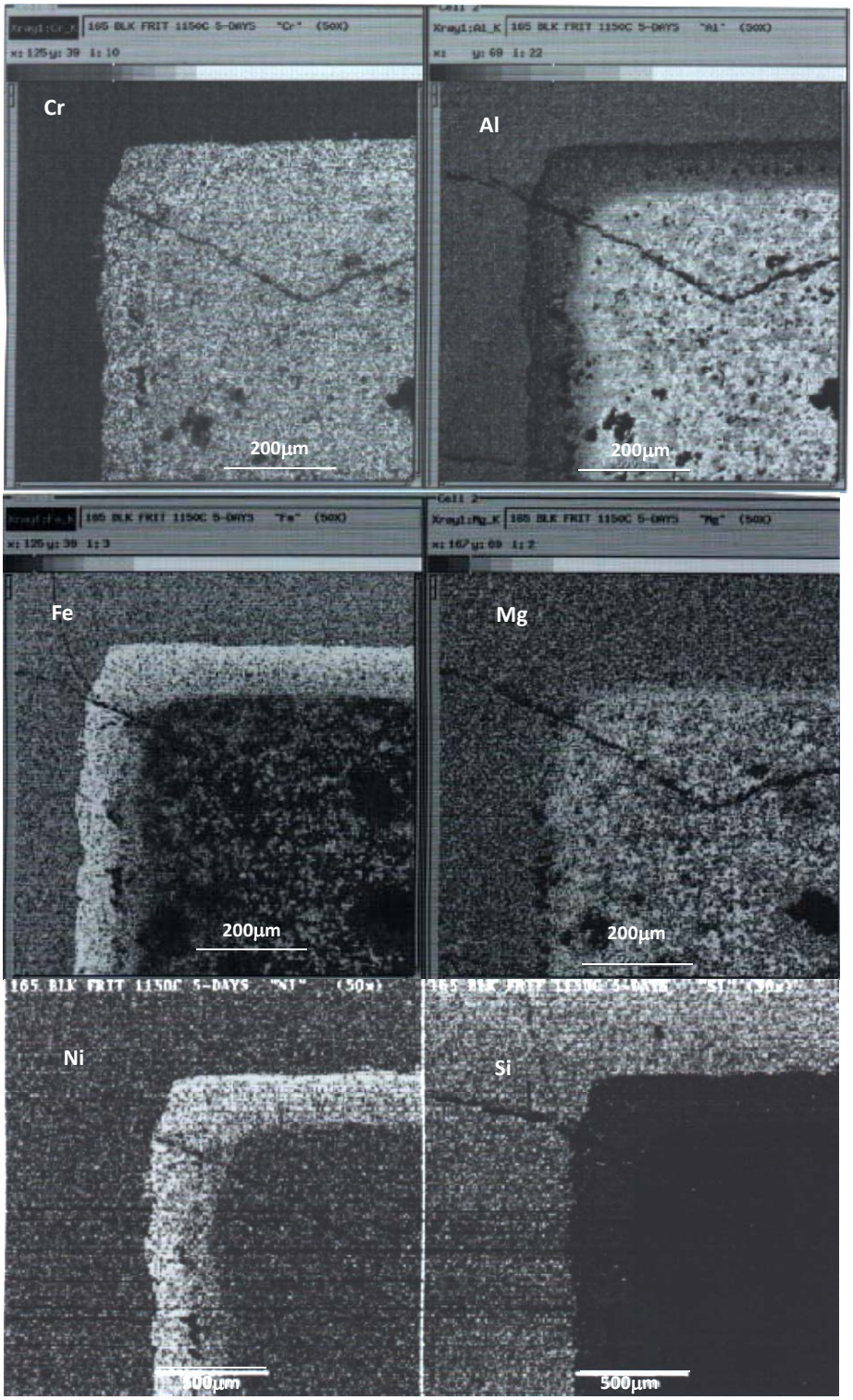

Figure 7. X-ray maps showing enrichment (brighter outer rim image) in Cr, Fe and Ni in the corrosion layer corresponding to Figure 6 and showing depletion (darker outer rim image) in Al, Mg, and Si the corrosion layer.

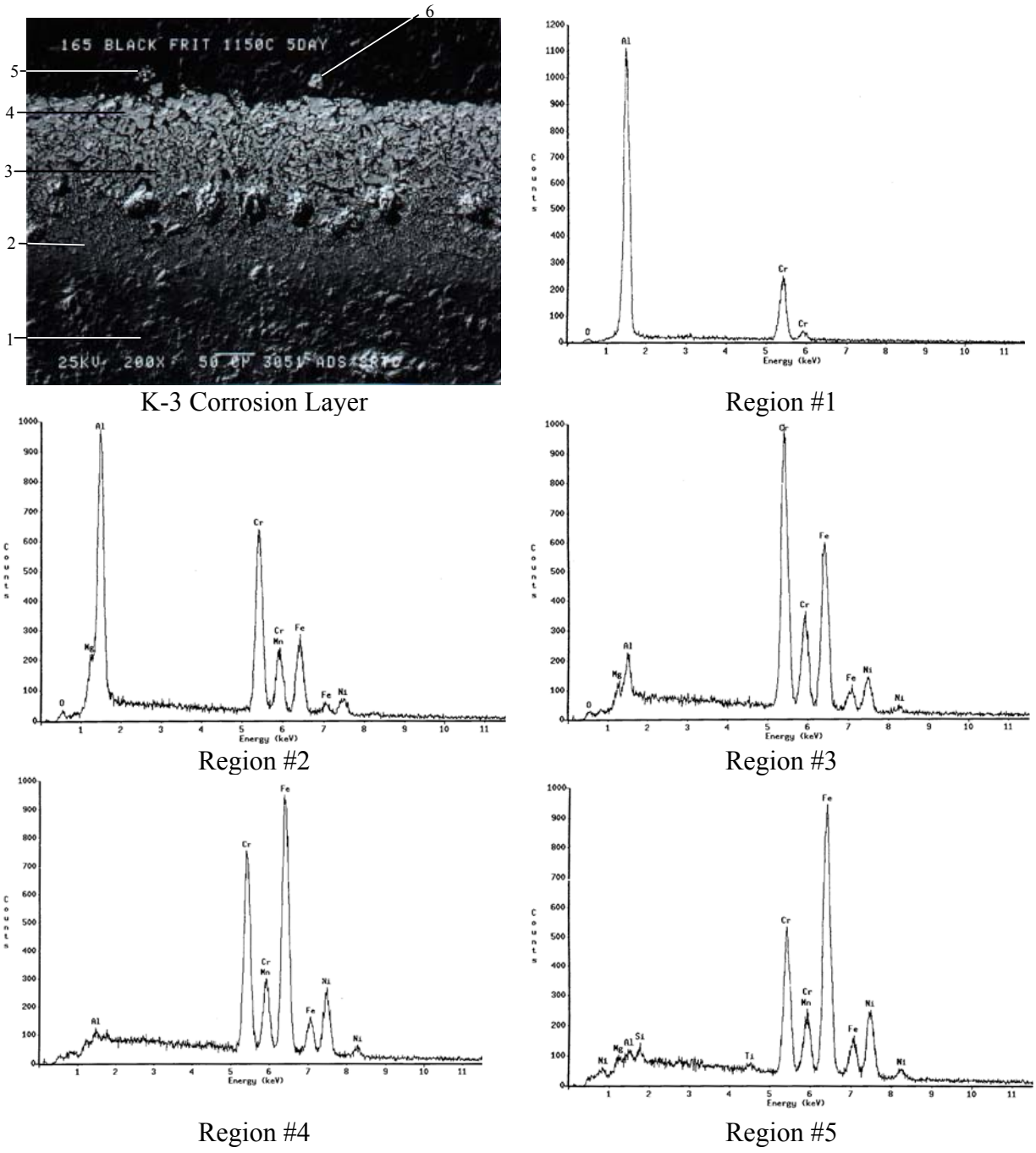

Figure 8. Enlargement of the corrosion layer showing the different morphologies of the corrosion layer (regions #3 and #4) separated from the penetration layer (regions #2) and the bulk K-3 (region #1). The bulk glass is indicated by region #5. Note the inclusion (region #6) that has broken off from the corrosion layer and is dissolving in the glass in Figure 9.

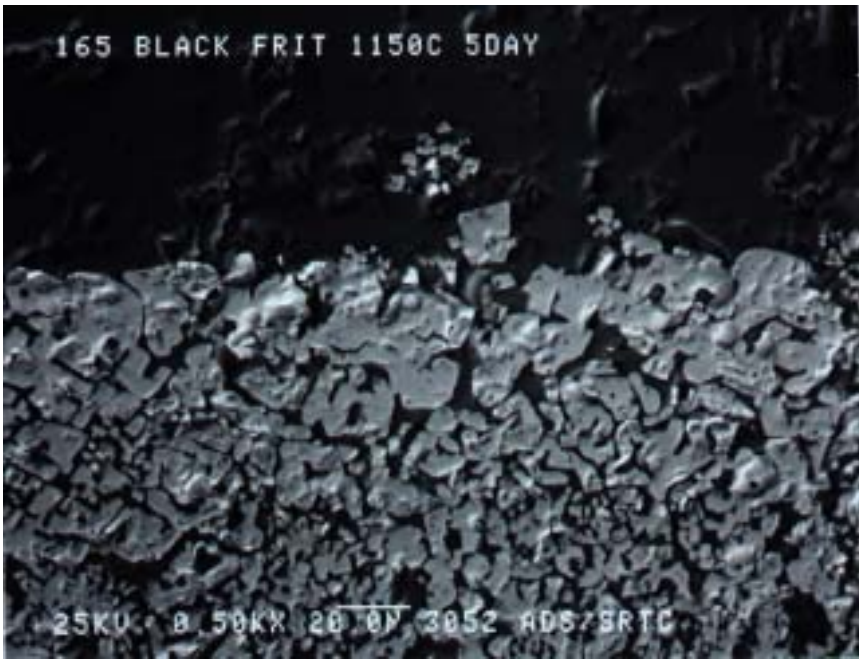

Figure 9. An enlarged Scanning Electron Micrograph of the outer corrosion layer (region 6 of Figure 8a) of the Monofrax ™ K-3 refractory, the breaking away of the Fe-Cr-Mn-Ni rich corrosion layer which is an insoluble $Ni,Mn(Fe,Cr)_2O_4$ rich spinel which may be adhere to the melter refractory wall or spall off and fall to the bottom of the melter creating bottom deposits.

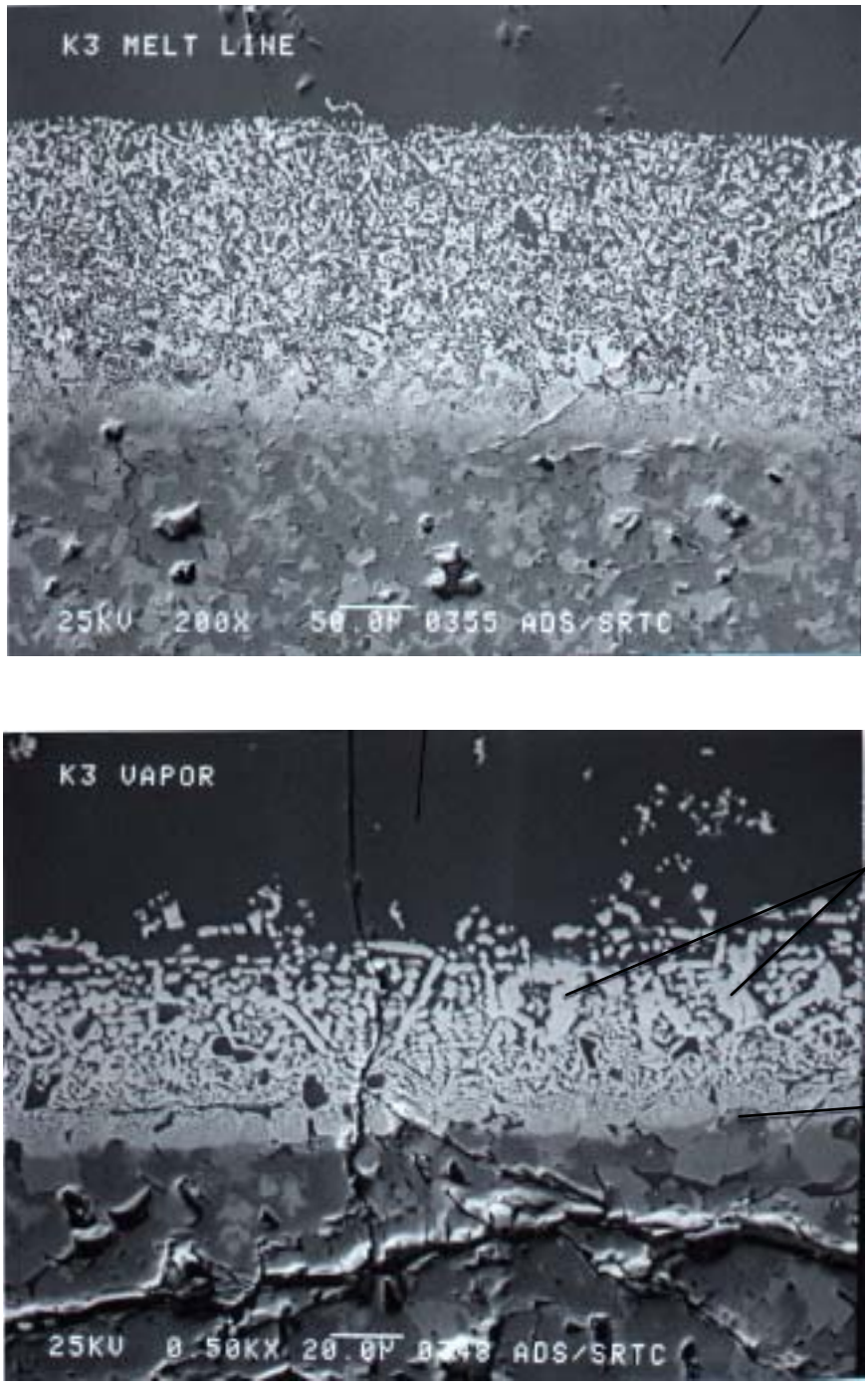

Figure 10. Monofrax™ K-3 corrosion coupons immersed in the SRNL mini-melter melt pool for 3 days at 1150°C in highly oxidized feed. The top figure shows corrosion at or near the melt line and the bottom figure shows corrosion experienced in the vapor space. Note the corrosion layer composes the largest fraction of the total penetration layer at the melt line, when compared to the other Monofrax™ K-3 coupons tested in the crucible melts (Table 5). This is probably due to the effects of convection causing erosion-corrosion and faster depletion of the corrosion layer in Al_2O_3.

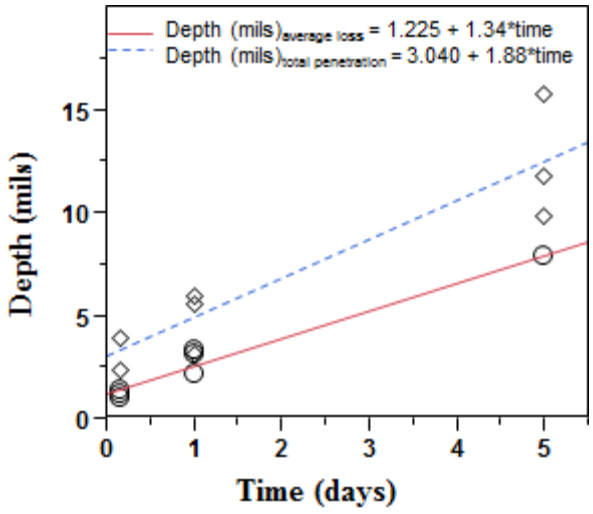

Figure 11. Linear Corrosion Rates of K-3 refractory measured as total penetration (mils) and average loss of material (mils) versus time in hours for replicates 1, 2, and 3. Note that the average outer loss values are more reproducible than the total penetration depths as the average outer loss values are easier to measure.

REFERENCES

1 Jantzen,C.M., Imrich, K.J., Brown, K.G., and Pickett, J.B., **"High Chrome Refractory Characterization: Part II. Accumulation of Spinel Corrosion Deposits in Radioactive Waste Glass Melters,"** International Journal of Applied Glass Science, this issue. (2014).

2 Certa, P.J. and M.N. Wells, **"River Protection Project System Plan,"** ORP-11242, Rev. 5, DOE Office of River Protection, Richland, WA (November 2010).

3 R.A. McCauley, **"Corrosion: A Review of Some Fundamentals,"** Corrosion of Materials by Molten Glass, G.A. Pecoraro, J.C. Marra, and J.T. Wenzel (Eds), Ceramic Transactions, V. 78, Am. Ceram. Soc., Westerville, OH, 81-87 (1996).

4 W.E. Lee and S. Zhang, **"Melt Corrosion of Oxide and Oxide-Carbon Refractories,"** Intl. Materials Reviews, 44[3], 77-104 (1999).

5 W.E. Lee and R.E. Moore, **"The Evolution of *in situ* Refractories in the 20th Century,"** J. Am. Ceram. Soc. 81 [6] 1385-1410 (1998).

6 W.N. Rankin, P.E. O'Rourke, P.D. Soper, M.B. Cosper, and B.C. Osgood, **"Evaluation of Corrosion and Deposition in the 1941 Melter,"** U.S. DOE Report DPST-82-231, E.I. duPont deNemours & Co., Savannah River Laboratory, Aiken, SC (March, 1982).

7 P.A. Bingham, A.J. Connelly, N.C. Hyatt, and R.J. Hand, **"Corrosion of Glass Contact Refractories for the Vitrification of Radioactive Wastes: A Review",** Intl Materials Reviews 56 [4] 226 (2011).

8 S.A. Degterov and A.D. Pelton, **"Thermodynamic Calculation of Glass/Slag/Refractory Equilibria in Coal Gassification,"** Corrosion of Materials by Molten Glass, G.A. Pecoraro, et.al. (Eds), Ceram. Trans., V. 78, Am. Ceram. Soc., Westerville, OH, 91-103 (1996).

9 M.J. Plodinec, **"Vitrification Chemistry and Nuclear Waste,"** J. Non-Cryst. Solids, 84, 206-214 (1986).

10 W.A. Miller and W.C. Steggs, **"Evolution and Application of Chrome Bearing Fused Cast Refractories,"** Carborundum Co, Flaconer, NY (1975) as cited in Reference 12.

11 C.M. Jantzen, K.G. Brown, K.J. Imrich, and J.B. Pickett, **"High Cr_2O_3 Refractory Corrosion in Oxidizing Melter Feeds: Relevance to Nuclear and Hazardous Waste Vitrification,"** Ceramic Transactions, v. 93, J.C. Marra and G.T. Chandler (Eds.), American Ceramic Society, Westerville, OH, 203-212 (1999).

12 D.C. Iverson and D.F. Bickford, **"Evaluation of Materials Performance in a Large-Scale Glass Melter After Two Years of Vitrifying Simulated SRP Defense Waste,"** Sci. Basis for Nucl. Waste Mgt., VIII, Mat. Res. Soc., Pittsburgh, PA, 839-845 (1985).

13 A. Muan and E.F. Osborn, **"Phase Equilibria Among Oxides in Steelmaking,"** Addison-Wesley Publishing Company, Inc., Reading, MA, 236pp. (1965).

14 G.L. Smith, D.K. Peeler, H.D. Smith, P .A. Smith, E.M. Tracey, and K.D. Wiemers, **"Effect of Feed Chemistry on Waste Melter Vitrification Kinetics,"** U.S. DOE Report, PVTD-T3C-95-129, Pacific Northwest Laboratory, Richland, WA (September, 1995).

15 S. Zhang and W.E. Lee, **"Use of Phase Diagrams in Studies of Refractories Corrosion,"** Intl. Materials Reviews. 45 [2] 41-58 (2000).

16 S.A. Cooper and P.S. Nicholson, **"Influence of Glass Redox Conditions on the Corrosion of Fusion-Cast Chrome-Alumina Refractories,"** Ceramic Bulletin, 59[7], 715-717 (1980).

17 W.E. Lee, S. Zhang, and H. Sarpoolaky, **"Different Types of *in situ* Refractories,"** Ceramic Transactions 125, American Ceramic Society, pp.245-252 (2001).

18 G.G. Wicks, **"Compatibility Tests of Materials for A Prototype Ceramic Melter for Defense Waste Products,"** Ceramics in Nuclear Waste Management, U.S. DOE Report CONF-790420, U.S. Dept. of Energy, Nat'l. Tech. Info. Service, Springfield, VA 82-85 (1979).

19 G.G. Wicks, **"Corrosion of Melter Materials,"** U.S. DOE Report DPST-79-580, E.I. duPont deNemours & Co., Savanannah River Laboratory, Aiken, SC (May, 1980).

20 W.N. Rankin, "**Evaluation of Glass-Contact Materials for Waste Glass Melters,"** Nuclear Waste Management, Advances in Ceramics, V. 8, G.G. Wicks and W.A. Ross (Eds.), Am. Ceram. Soc., Westerville, OH, 559-566 (1984).

21 W.N. Rankin, **"Corrosion of Melter Materials: Part III. Effect of Na_2O,"** U.S. DOE Report DPST-81-933, E.I. duPont deNemours & Co., Savanannah River Laboratory, Aiken, SC (February, 1982).

22 H.D. Schreiber and E.V. Sampson, Jr., **"A Corrosion Model for Metals in Molten Glass,"** Corrosion of Materials by Molten Glass, G.A. Pecoraro, J.C. Marra, and J.T. Wenzel (Eds), Ceramic Transactions, V. 78, Am. Ceram. Soc., Westerville, OH, 91-103 (1996).

23 G.G. Wicks, **"Melter Materials Compatibility Program, Part I: Static and Dynamic Finger Tests-Simulated Glass Waste,"** U.S. DOE Report DPST-78-465, E.I. duPont deNemours & Co., Savanannah River Laboratory, Aiken, SC (August, 1978).

24 G.G. Wicks, **"Melter Materials Compatibility Program, Part II: Static and Dynamic Finger Tests, Radioactive Waste Glass and Long-Term Simulated Tests,"** U.S. DOE Report DPST-79-526, E.I. duPont deNemours & Co., Savanannah River Laboratory, Aiken, SC (November, 1979).

25 Corning Engineering Laboratory Services Report for W.N. Rankin, #11988-008 (July 31, 1985).

26 C.M. Jantzen, F.C. Johnson, M.E. Stone, D.C. Koopman, J.R. Zamecnik, K.G. Brown, J.B. Pickett, and C.C. Herman, **"Melter REDuction/OXidation (REDOX) Control to Optimize Melting and Retain Radionuclides: Part I. High Level Waste Melter REDOX Requirements and Measurement,"** (in preparation for IJAGS).

27 E.W. Baumann, **"Colorimetric Determination of Iron (II) and Iron (III) in Glass,"** Analyst, 117, 913-916 (1992).

28 H. Sarpoolaky, S. Zhang and W. E. Lee, **"Corrosion of High-Alumina and Near-Stoichiometric Spinels in Iron-containing Silicate Slags",** J. Euro. Ceram. Soc. 23 [2] 293-300 (2003)

29 C.M. Jantzen and D.P. Lambert, **"Inspection and Analysis of the Integrated DWPF Melter System (IDMS) After Seven Years of Operation,"** U.S. DOE Report WSRC-RP-575, Westinghouse Savannah River Co., Aiken, SC (February, 1997).

30 I. Barin, **"Thermochemical Data of Pure Substances, Parts 1 and 2,"** VCH Publishers, NY, NY, 1739pp (1989).

31 M.J. LaMont and P. Hrma, **"A Crucible Study of Spinel Settling in a A High-Level Waste Glass,"** Ceramic Trans. V. 87, 343-348 (1998).

32 J. Klouzek, J. Alton, P. Hrma, and T. Plaisted, **"Crucible Study of Spinel Settling in Molten High-Level Waste Glass,"** Ceramic Trans. V. 119, 301-308 (2001)

33 J.W. Amoroso, D.K. Peeler, and T.B. Edwards, **"Elimination of the Characterization of DWPF Pour Stream Sample and the Glass Fabrication and Testing of the DWPF Sludge Batch Qualification Sample,"** U.S. DOE Report SRNL-STI-2012-00157, Rev.0, Savannah River National Laboratory, Aiken, SC (2012).

34 M.J. Sienko and R.A. Plane, **Chemistry**, McGraw Hill, New York 623pp (1961)

35 C.M. Jantzen and M.E. Stone, **"Role of Manganese Reduction/Oxidation (REDOX) on Foaming and Melt Rate in High Level Waste (HLW) Melters,"** U.S. DOE Report WSRC-STI-2006-00066, Westinghouse Savannah River Co. (2007).

36 M.M. Reigel, **"Literature Review: Assessment of DWPF Melter Lifetime,"** U.S. DOE Report SRNL-STI-2014-00134, Savannah River National Laboraoty, Aiken, SC (2014).

37 C.M. Jantzen, C.M. **"Development of Glass Matrices for HLW Radioactive Wastes,"** in Handbook of Advanced Radioactive Waste Conditioning Technologies, M. Ojovan (Ed.), Woodhead Publishing, Oxford, 230-292 (2011).

38 D.F. Bickford, A.A. Ramsey, C.M. Jantzen, and K.G. Brown, **"Control of Radioactive Waste Glass Melters: I. Preliminary General Limits at Savannah River,"** J. Am. Ceram. Soc., 73[10], 2896-2902 (1990).

39 D.K. Peeler and C.M. Jantzen, **"Process Control Limits For Poorly Soluble Species In Borosilicate and Soda-Lime-Silica Glasses,"** U.S. DOE Report (in draft).

40 W. Volf, **"Glass Science and Technology, 7: Chemical Approach to Glass,"** Elsevier Scientific Publishers, New York (1984).

41 C.M. Jantzen and K.G. Brown, **"Predicting the Spinel-Nepheline Liquidus for Application to Nuclear Waste Glass Processing: Part I. Primary Phase Analysis, Liquidus Measurement, and Quasicrystalline Approach,"** J. Am. Ceramic Soc., 90 [6], 1866-1879 (2007).

42 C.M. Jantzen and K.G. Brown, **"Predicting the Spinel-Nepheline Liquidus for Application to Nuclear Waste Glass Processing: Part II. Quasicrystalline Freezing Point Depression Model,"** J. Am. Ceramic Soc. 90 [6], 1880-1891 (2007).

43 S.O Bates and W.M. Bowen, **"Report on Composition Variation Testing Conducted for Hanford Waste Vitrification,"** HWVP-86-V1122C, Pacific Northwest Laboratory, Richland, WA (1987).

44 J.M. Perez and R.W. Nakaoka, **"Vitrification Testing of Simulated High-Level Radioactive Waste from Hanford,"** Waste Management '86, R.G. Post (Ed.), Proceedings of the Symposium in Waste Management at Tuscon, AZ, March 2-6, 1986, 495-505 (1986).

45 H.D. Schreiber and A.L. Hockman, **"Redox Chemistry in Candidate Glasses for Nuclear Waste Immobilization,"** J. Am. Ceram. Soc., 70[8], 591-594

46 J. Sussmilch and A. Jouan, **"The Vitrification of Accident Wastes from the Nuclear Power Plant A-1 in Slovakia,"** Proceedings of Environemental Remediation and Environmental Issues, Vol. 3 (1993).

47 "**Handbook of Chemistry and Physics**," 54th Edition, CRC Press, Cleveland, OH (1973).

48 A.S. Choi, **"Maximum Total Organic Carbon Limit for DWPF Melter Feed,"** U.S. DOE Report WSRC-TR-95-0119, Rev. 0, Westinghouse Savannah River Company, Aiken, SC (March 13, 1995).